Synthesis, Crystal Structure, and Optical and Thermal Properties of $(C_4H_9NH_3)_2MI_4$ (M = Ge, Sn, Pb)

David B. Mitzi

IBM T. J. Watson Research Center, P.O. Box 218, Yorktown Heights, New York 10598

Received October 24, 1995. Revised Manuscript Received January 8, 1996[⊗]

Single crystals of the organic-inorganic layered perovskites $(C_4H_9NH_3)_2MI_4$ (M = Ge, Sn, Pb) have been grown from aqueous hydriodic acid solutions. X-ray diffraction, thermal analysis, and photoluminescence spectroscopy were used to compare crystal structure, metal atom lone-pair stereoactivity, and physical properties as a function of group IVB element. The orthorhombic $(C_4H_9NH_3)_2GeI_4$ structure, refined in the space group *Pcmn*, consists of single-layer-thick perovskite sheets of distorted corner-sharing GeI_6 octahedra separated by *n*-butylammonium cation bilayers. $(C_4H_9NH_3)_2SnI_4$ and $(C_4H_9NH_3)_2PbI_4$ are structurally very similar but adopt the space group *Pbca*, with a more ideal octahedral iodine coordination around the divalent group IVB atoms. Within the more general tin(II)-based family, $(C_4H_9NH_3)_2(CH_3NH_3)_{n-1}Sn_nI_{3n+1}$, a structural comparison between the title semiconducting $n = 1$ compound and the previously reported semimetallic $n = 3$ and metallic $n \rightarrow \infty$ members demonstrates a correlation between perovskite sheet thickness, Sn(II) lone-pair stereochemical activity, average Sn−I bond length, and electrical conductivity within this series. While $(C_4H_9NH_3)_2GeI_4$ melts at 222(2) °C, significantly below its bulk decomposition temperature, $(C_4H_9NH_3)_2SnI_4$ (T_m = 256(2) °C) and $(C_4H_9NH_3)_2PbI_4$ (T_m = 285(4) °C) melt/decompose at progressively higher temperatures and are less stable as a melt. Room-temperature photoluminescence from the title compounds exhibits a pronounced spectral peak in the visible range, with the peak wavelength varying between 690(5), 625(1), and 525(1) nm for the M = Ge, Sn, and Pb compounds, respectively.

Introduction

Hybrid organic−inorganic materials offer scientifically and technologically significant opportunities for combining attractive features of inorganic and organic systems within a single material. While inorganic materials offer the potential for high carrier density and mobility, interesting magnetic or ferroelectric transitions, and substantial thermal stability, organic materials provide virtually unlimited flexibility to choose molecules of varying length, width, polarizability, and degree of saturation or polymerization, as well as offering exceptional luminescent properties and the potential for conductivity (even superconductivity). Useful integration of organic and inorganic components within a "tailored" hybrid material has already been demonstrated by the artificial layering of TiO_x and copper phthalocyanine (CuPc) within an organic−inorganic heteromultilayer structure.[1] Under illumination, charge carrier photogeneration primarily occurs in the CuPc layers, while the higher mobility TiO_x layers transport the electrons in-plane after charge separation at the interface, leading to 40 times higher photoconductivity than in a CuPc single layer.

In addition to artificially prepared organic−inorganic hybrid materials, considerable interest has also been focused on self-organizing organic−inorganic systems. A fairly extensive class,[2] with composition A_2MX_4, consists of alternating layers of single metal halide (MX_4^{2-}) perovskite sheets and organic ammonium cation (A^+) bilayers, and are particularly interesting because of the ability to use the organic layers to control properties of the inorganic perovskite sheets. With first-row transition-metal halides, for example, the systems are interesting candidates for the study of lower dimensional magnetism,[3−5] since control over coupling between magnetic metal halide layers is provided by the flexibility to choose alkyl chain length in the organic layer separating the magnetic layers.

Recently, the divalent group IVB metal halide members of the organic−inorganic perovskite family have been synthesized and have generated considerable interest as self-assembling multi-quantum-well structures. $(C_4H_9NH_3)_2(CH_3NH_3)_{n-1}Sn_nI_{3n+1}$ ($n = 1-5$) forms a series of conducting layered organic−inorganic perovskites consisting of *n* ⟨100⟩-terminated conducting $CH_3NH_3SnI_3$ perovskite sheets alternating with insulating bilayers of butylammonium cations.[6] As *n* increases, the materials undergo a semiconductor−metal transition, with the end-member cubic perovskite, $CH_3NH_3SnI_3$, found to be a low-carrier-density p-type metal.[7] Besides a simple alkyl chain, more complicated organic cations can also be incorporated, including the phenethylammonium cation.[6,8,9] Replacement of the butyl-

[⊗] Abstract published in *Advance ACS Abstracts,* February 15, 1996.

(1) Takada, J.; Awaji, H.; Koshioka, M.; Nakajima, A.; Nevin, W. A. *Appl. Phys. Lett.* **1992**, *61*, 2184.
(2) Arend, H.; Huber, W.; Mischgofsky, F. H.; Richter-Van Leeuwen, G. K. *J. Cryst. Growth* **1978**, *43*, 213.
(3) de Jongh, L. J.; Botterman, A. C.; de Boer, F. R.; Miedema, A. R. *J. Appl. Phys.* **1969**, *40*, 1363.
(4) de Jongh, L. J.; Miedema, A. R. *Adv. Phys.* **1974**, *23*, 1.
(5) Rubenacker, G. V.; Haines, D. N.; Drumheller, J. E.; Emerson, K. *J. Magn. Magn. Mater.* **1984**, *43*, 238.
(6) Mitzi, D. B.; Feild, C. A.; Harrison, W. T. A.; Guloy, A. M. *Nature* **1994**, *369*, 467.
(7) Mitzi, D. B.; Feild, C. A.; Schlesinger, Z.; Laibowitz, R. B. *J. Solid State Chem.* **1995**, *114*, 159.

0897-4756/96/2808-0791$12.00/0

ammonium cation with indoformamidinium stabilizes a new layered organic−inorganic structural family,[10] represented by $[NH_2C(I)=NH_2]_2(CH_3NH_3)_mSn_mI_{3m+2}$, consisting of m perovskite sheets terminating on a ⟨110⟩ surface (rather than the usual ⟨100⟩ termination) and demonstrating the ability to control crystallographic orientation of the perovskite sheets through the choice of organic cation. The $m = 1$ member of this family is particularly notable[11] since the layered perovskite framework is reduced to a network of quasi-one-dimensional "perovskite chains", providing the possibility to synthesize one ($m = 1$), two ($m \geq 2$), and three ($m \rightarrow \infty$) dimensional structures within this organic−inorganic layered perovskite family.

In addition to the unusually high conductivity in the tin(II) iodides, the lead(II)-based organic−inorganic layered perovskites have demonstrated enhanced exciton binding energies due to a dielectric confinement effect,[12,13] nonlinear optical properties with the potential for third harmonic generation,[14,15] and electroluminescence.[16] Recently, a heterostructure electroluminescent device using $(C_6H_5C_2H_4NH_3)_2PbI_4$ as an emitter material has been demonstrated,[17] producing highly intense green electroluminescence of more than 10 000 cd m^{-2} (at liquid nitrogen temperature) with a current density of 2 A cm^{-2}. While significant results have been presented on the Sn(II)- and Pb(II)-based systems, only passing mention has been made of the Ge(II) organic−inorganic layered systems,[18] presumably because of the decreasing stability of the group IVB divalent state progressing up the periodic table in this family. The three-dimensional perovskites, $AGeX_3$ (A = Rb, Cs; X = Cl, Br, I), however, have been synthesized and characterized structurally and electrically.[19,20] $CsGeI_3$ is particularly interesting, given its metallic character, similar to that of some of the Sn(II) halide perovskites.

In this paper, we present a low-temperature (below 100 °C) aqueous solution growth technique for preparing single crystals of the $n = 1$ member of the Ge(II) ⟨100⟩-oriented layered organic−inorganic perovskites, $(C_4H_9NH_3)_2GeI_4$, along with a detailed single-crystal structure refinement, thermogravimetric, and differential thermal analysis and photoluminescence measurements for this compound. The tin(II) and lead(II) analogue are also presented, providing an opportunity to study the progression of physical and chemical properties as a function of metal atom in the group IVB column of the periodic table. In the more general Sn(II)-based family, $(C_4H_9NH_3)_2(CH_3NH_3)_{n-1}Sn_nI_{3n+1}$, only the structures of the semimetallic $n = 3$ and the metallic $n \rightarrow \infty$ compounds have been previously reported.[6] Comparison of these structures with the present semiconducting $n = 1$ structure provides an opportunity to examine a possible structural basis for the semiconductor−metal transition observed in this family,[6] as well as to examine the effect of Sn(II) lone-pair stereoactivity as a function of increasing perovskite sheet thickness and conductivity.

Experimental Section

Synthesis. Crystals of the title compounds were grown from slowly cooled aqueous hydriodic acid solutions, with all synthetic steps and crystal manipulations after synthesis being performed in an inert atmosphere to prevent oxidation. For $(C_4H_9NH_3)_2GeI_4$, 0.709 g (1.22 mmol) of GeI_4 was dissolved in 50 mL 3 M HI solution at 80 °C. The temperature of the solution was raised to 98 °C and 4 mL concentrated (50 wt %) aqueous H_3PO_2 solution was added. After allowing the reduction of GeI_4 to GeI_2 to proceed for approximately 4 h, a solution of 0.491 g (2.44 mmol) of $(C_4H_9NH_2)\cdot HI$ in 3 mL of concentrated (57 wt %) aqueous HI was added, producing a yellow solution. The resulting solution was allowed to sit at 80 °C in flowing argon until approximately 50% of the solution had evaporated and then slowly (2−5 °C/h) cooled to −10 °C. The bright orange sheetlike crystals were filtered under flowing argon and dried in argon at 80 °C.

Crystals of $(C_4H_9NH_3)_2SnI_4$ and $(C_4H_9NH_3)_2PbI_4$ were grown using a technique described earlier[6,7] for the related $(C_4H_9NH_3)_2(CH_3NH_3)_{n-1}Sn_nI_{3n+1}$ compounds. Briefly, 0.481 g (1.29 mmol) of SnI_2 or 0.534 g (1.16 mmol) of PbI_2 was dissolved in 2 mL of concentrated (57 wt %) aqueous HI solvent under flowing argon at 90 °C. In a separate tube, a stoichiometric quantity (i.e., 2.58 mmol for the Sn system and 2.32 mmol for the Pb system) of $(C_4H_9NH_2)\cdot HI$ was dissolved in 3 mL of concentrated HI solution and was then added to the metal halide solution. After ramping the solution temperature at 2 °C/h from 90 to −10 °C, the crystals formed were filtered under argon or nitrogen and dried in argon at 80 °C. The sheetlike crystals of the single-layer tin compound are dark red, while those of the lead compound are orange-yellow.

X-ray Crystallography. Suitable single crystals were selected in an argon-filled drybox (<1 ppm O_2 and H_2O) under a microscope and sealed in quartz capillaries. Data for each of the title compounds were collected at room temperature on an Enraf-Nonius CAD4 diffractometer with graphite-monochromatized Mo Kα radiation. The data collection parameters and the structural refinement results are tabulated in Table 1. The unit-cell parameters and the crystal orientation matrix were obtained by a least-squares fit of 25 reflections with 18° < 2θ < 30°. Intensity control reflections were monitored every 5000 s during the data collection. Very little degradation (approximately 3% drop in the intensity control reflections over a total exposure time of 140 h) was noted and accounted for during data analysis for the germanium compound, while no observable degradation was observed for either the tin or lead com-

(8) Mitzi, D. B. *Bull. Am. Phys. Soc.* **1993**, *38*, 116.
(9) Papavassiliou, G. C.; Koutselas, J. B.; Lagouvardos, D. J. *Z. Naturforsch.* **1993**, *48b*, 1013.
(10) Mitzi, D. B.; Wang, S.; Feild, C. A.; Chess, C. A.; Guloy, A. M. *Science* **1995**, *267*, 1473.
(11) Wang, S.; Mitzi, D. B.; Feild, C. A.; Guloy, A. *J. Am. Chem. Soc.* **1995**, *117*, 5297.
(12) Ishihara, T.; Takahashi, J.; Goto, T. *Solid State Commun.* **1989**, *69*, 933.
(13) Hong, X.; Ishihara, T.; Nurmikko, A. V. *Phys. Rev. B* **1992**, *45*, 6961.
(14) Xu, C.; Kondo, T.; Sakakura, H.; Kumata, K.; Takahashi, Y.; Ito, R. *Solid State Commun.* **1991**, *79*, 245.
(15) Calabrese, J.; Jones, N. L.; Harlow, R. L.; Thorn, D.; Wang, Y. *J. Am. Chem. Soc.* **1991**, *113*, 2328.
(16) Hong, X.; Ishihara, T.; Nurmikko, A. V. *Solid State Commun.* **1992**, *84*, 657.
(17) Era, M.; Morimoto, S.; Tsutsui, T.; Saito, S. *Appl. Phys. Lett.* **1994**, *65*, 676.
(18) Papavassiliou, G. C.; Koutselas, I. B. *Synth. Met.* **1995**, *71*, 1713.
(19) Guen, L.; Palvadeau, P.; Spiesser, M.; Tournoux, M. *Rev. Chim. Miner.* **1982**, *19*, 1.
(20) Thiele, G.; Rotter, H. W.; Schmidt, K. D. *Z. Anorg. Allg. Chem.* **1987**, *545*, 148.

Table 1. Data Collection and Structure Refinement Parameters for $(C_4H_9NH_3)_2MI_4$ (M = Ge, Sn, Pb)

formula	$(C_4H_9NH_3)_2GeI_4$	$(C_4H_9NH_3)_2SnI_4$	$(C_4H_9NH_3)_2PbI_4$
formula weight	728.499	774.599	863.109
crystal color	orange	red	orange
crystal system	orthorhombic	orthorhombic	orthorhombic
space group	*Pcmn*	*Pbca*	*Pbca*
a, Å	8.7220(5)	8.8370(5)	8.8632(21)
b, Å	8.2716(4)	8.6191(4)	8.6816(8)
c, Å	28.014(1)	27.562(2)	27.570(2)
V, Å	2021.1(2)	2099.3(2)	2121.4(6)
Z	4	4	4
ϱ_{calcd}, g/cm^3	2.394	2.451	2.702
radiation (λ), Å	Mo Kα (0.7093)	Mo Kα (0.7093)	Mo Kα (0.7093)
absorption coefficient (μ), cm^{-1}	75.3	70.3	137.7
transmission factor range	0.591−1.000	0.699−1.000	0.685−1.000
scan mode	$\omega-2\theta$	$\omega-2\theta$	$\omega-2\theta$
2θ range, deg	$4.8 \le 2\theta \le 50.0$	$4.0 \le 2\theta \le 50.0$	$4.0 \le 2\theta \le 50.0$
data collected	$\pm h, k, \pm l$	$\pm h, \pm k, l$	$\pm h, \pm k, l$
no. of data collected	7231	6642	6793
no. of unique data	1910	1847	1873
no. of data used in refinement	1387 ($I > 3\sigma(I)$)	1242 ($I > 3\sigma(I)$)	1081 ($I > 3\sigma(I)$)
no. of variables	58	45	45
R_F[a]	0.053	0.048	0.050
R_w[b]	0.051	0.056	0.054

[a] $R_F = \sum(F_o - F_c)/\sum(F_o)$. [b] $R_w = \{\sum w(F_o - F_c)^2/\sum(wF_o^2)\}^{1/2}$.

pounds. Empirical absorption corrections based on several azimuthal scans were also applied. The NRCVAX 386 PC version[21] program was used for the structural solution and refinement.

The space group *Pbca* (No. 61) was chosen for both the tin and lead compounds based on the observation of the systematic reflection conditions $0kl$, $k = 2n$; $h0l$, $l = 2n$; and $hk0$, $h = 2n$ and the successful structural refinements. For $(C_4H_9NH_3)_2GeI_4$, the space group *Pcmn* (No. 62) was chosen because of the systematic absences $0kl$, $l = 2n$; $hk0$, $h + k = 2n$; $h00$, $h = 2n$; $0k0$, $k = 2n$; and $00l$, $l = 2n$. The nonstandard setting *Pcmn* was used rather than *Pmna* in order to keep the axes in the same configuration as for the tin and lead compounds. While the structure for the germanium compound could also be successfully refined in the noncentrosymmetric space group $Pc2_1n$ (No. 33), with slight reductions in the *R* factors, the centrosymmetric space group was finally selected because the acentric solution demonstrated considerable instability during refinement, the thermal parameters for the centric refinement were well behaved, and analysis of the *E* statistics favored this choice ($|E^2 - \mathbf{1}| = 1.216$, experimental; 0.968, theoretical centric; 0.736, theoretical acentric). Furthermore, the heavy-atom positions and thermal parameters were very similar in both space groups, providing no incentive to adopt the acentric cell. The only concrete evidence perhaps suggesting the acentric cell are significantly smaller thermal parameters for the organic component of the structure in this space group (for example, the B_{iso} for N(1)/N(2) are 11.5(8)/12.3(9) versus 6.8(6)/7.6(7) for refinements in *Pcmn* and $Pc2_1n$, respectively). Measurement of optical activity, piezoelectricity, or other phenomena which are sensitive to center of symmetry, is needed to unambiguously establish whether the true space group for this compound is centrosymmetric or whether this just approximates the true symmetry.

The positions of the heavy atoms (Ge, Sn, Pb, and I) were determined by direct methods, while the remaining non-hydrogen atomic positions were picked up from the Fourier difference maps. Locating the hydrogen atoms was not attempted. All the heavy atoms were refined anisotropically, while the light nitrogen and carbon atoms were refined isotropically. The relatively large carbon thermal parameters and the presence of several anomalously small carbon−carbon bond distances (i.e., 1.1(1) Å), especially near the ends of the butyl chains, suggest either significant thermal motion or the existence of some disorder within the organic layers of the structures. The minimum and maximum electron densities in the final difference Fourier syntheses were −1.320, −1.440, −1.290 e/A^3 and 1.810, 1.170, 1.310 e/A^3 for the Ge, Sn, and Pb compounds, respectively. The atomic positions and isotropic thermal parameters for the germanium, tin, and lead compounds are tabulated in Tables 2−4, respectively. The anisotropic temperature factors for each title compound are supplied as supporting information (Tables S.1−S.3).

Table 2. Positional and Thermal Parameters[a] for $(C_4H_9NH_3)_2GeI_4$

atom	position	*x*	*y*	*z*	B_{iso} (Å^2)
Ge	4c	0.5095(2)	0.25	0.2478(1)	5.3(1)
I(1)	4c	0.4458(2)	0.25	0.1420(1)	6.95(9)
I(2)	8d	0.7332(1)	0.4969(1)	0.23800(4)	6.76(5)
I(3)	4c	0.5462(2)	0.25	0.35638(6)	7.2(1)
N(1)	4c	0.448(3)	0.75	0.164(1)	11.5(8)
N(2)	4c	0.043(4)	0.25	0.165(1)	12.3(9)
C(1)	4c	0.562(8)	0.75	0.123(3)	20(2)
C(2)	4c	0.514(8)	0.75	0.082(3)	20(2)
C(3)	4c	0.64(1)	0.75	0.045(3)	23(3)
C(4)	4c	0.596(8)	0.75	0.007(3)	23(3)
C(5)	4c	0.925(6)	0.25	0.126(2)	16(2)
C(6)	4c	0.982(6)	0.25	0.082(2)	16(2)
C(7)	4c	0.857(9)	0.25	0.047(3)	24(3)
C(8)	4c	0.904(8)	0.25	0.006(3)	22(3)

[a] Heavy atoms (Ge and I) are refined anisotropically; anisotropic thermal parameters are found in Table S.1 (supporting information).

Thermal Analysis. Simultaneous thermogravimetric analysis (TGA) and differential thermal analysis (DTA) were performed on the three title systems, using a Setaram TAG 24 thermal analysis system, to examine the thermal stability of each system. Approximately

(21) Gabe, E. J.; Le Page, Y.; Charland, J.-P.; Lee, F. L.; White, P. S. *J. Appl. Cryst.* **1989**, *22*, 384.

Table 3. Positional and Thermal Parameters[a] for $(C_4H_9NH_3)_2SnI_4$

atom	position	*x*	*y*	*z*	B_{iso} (Å^2)
Sn	4a	0.0	0.0	0.0	4.28(7)
I(1)	8c	0.0376(2)	0.0133(2)	0.1140(1)	6.83(7)
I(2)	8c	0.2081(1)	−0.2937(1)	−0.0062(1)	6.22(7)
N(1)	8c	0.077(2)	0.433(2)	0.0866(8)	8.7(5)
C(1)	8c	−0.050(4)	0.531(4)	0.118(1)	12(1)
C(2)	8c	−0.013(4)	0.510(5)	0.173(1)	14(1)
C(3)	8c	−0.143(5)	0.606(6)	0.194(2)	17(2)
C(4)	8c	−0.113(6)	0.585(6)	0.240(2)	20(2)

[a] Heavy atoms (Sn and I) are refined anisotropically; anisotropic thermal parameters are found in Table S.2 (supporting information).

Table 4. Positional and Thermal Parameters[a] for $(C_4H_9NH_3)_2PbI_4$

atom	position	*x*	*y*	*z*	B_{iso} (Å^2)
Pb	4a	0.0	0.0	0.0	4.91(5)
I(1)	8c	0.0338(2)	0.0152(3)	0.1154(1)	7.1(1)
I(2)	8c	0.1969(2)	−0.3052(2)	−0.0043(1)	6.6(1)
N(1)	8c	0.078(3)	0.425(3)	0.0936(8)	7.2(6)
C(1)	8c	−0.031(5)	0.539(5)	0.118(2)	13(1)
C(2)	8c	−0.020(6)	0.519(6)	0.170(2)	14(1)
C(3)	8c	−0.138(8)	0.601(9)	0.198(3)	21(3)
C(4)	8c	−0.114(8)	0.615(8)	0.237(3)	20(3)

[a] Heavy atoms (Pb and I) are refined anisotropically; anisotropic thermal parameters are found in Table S.3 (supporting information).

50−90 mg of sample were loaded into a tantalum container for each run, which consisted of a 2 °C/min ramp from 25 to 325 °C and back to 25 °C in an argon atmosphere. Special care was taken to exclude oxygen from the apparatus by evacuating and backfilling the thermal analysis apparatus with argon several times. The temperature was calibrated using the melting transitions of indium (T_m = 156.6 °C) and tin (T_m = 231.9 °C) using the same system configuration (crucible type, temperature ramp rate, gas type, gas flow, etc.). The reversibility of each transition was also checked by ramping up and down in temperature through each observed endotherm or exotherm.

Photoluminescence. Flat sheetlike crystals, with in-plane dimensions of several millimeters, were used to obtain the photoluminescence spectra. In some cases, the samples consisted of several crystals stacked up along the *c* axis, with good *c*-axis orientation but some misorientation in the *a*−*b* plane. The photoluminescence spectra were collected within several hours after the crystals were synthesized, and samples were maintained in an argon-filled cell during measurement to prevent degradation. Crystals left out in air for several hours showed clear signs of tarnishing (especially for the M = Ge and Sn samples). The photoluminescence spectra were excited by 457.9 nm (2.71 eV) light from an argon ion laser. This light was strongly absorbed by each sample, ensuring that the observed luminescence came from the front side of the samples. The excitation density was below 1 W cm^{-2}. The luminescence was analyzed by a triple monochromator and detected by a liquid nitrogen cooled CCD. The triple monochromator provided ample rejection of elastically scattered light, although the broad-band spectra of these materials had to be obtained over several separate spectral regions. Each individual spectrum was accumulated over a few seconds.

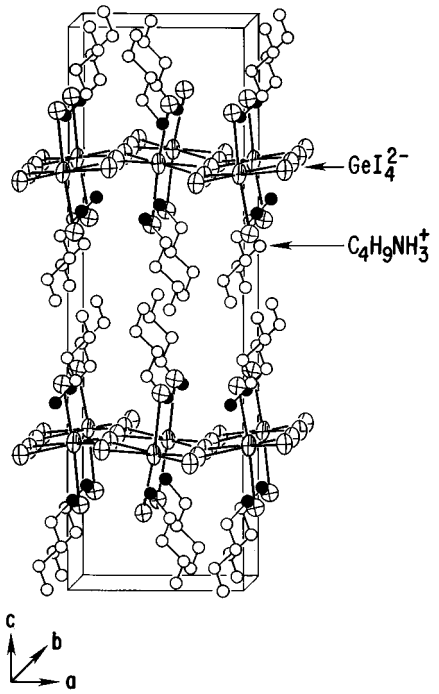

Figure 1. Unit cell of $(C_4H_9NH_3)_2GeI_4$ viewed along the *b* axis, with the unit cell outlined, highlighting the slight corrugation of the GeI_4 sheets along the *a* axis and the configuration of the butylammonium cations. The $(C_4H_9NH_3)_2SnI_4$ and $(C_4H_9NH_3)_2PbI_4$ structures are very similar (after a shift of origin) with, however, subtle differences in bonding within the MI_4 sheets and with the orientation of the butylammonium cations (see also the text and Figure 3). The thermal ellipsoids for germanium and iodine are drawn at 50% probability, while the carbon and nitrogen sphere sizes are arbitrary.

Results and Discussions

Structural Description. The orthorhombic structures for $(C_4H_9NH_3)_2MI_4$ (M = Ge, Sn, and Pb) each consist of single MI_4^{2-} infinite sheets of corner-shared MI_6 octahedra, separated by bilayers of *n*-butylammonium cations, with the ammonium group hydrogen/ionic bonding to halogens in the inorganic sheets and the butyl chains extending into the space between the layers (Figure 1). The relatively weak van der Waals force between the alkyl chains separating the layers provides for a highly two-dimensional structure. The metal halide sheets are derived from the three-dimensional $(CH_3NH_3)MI_3$ perovskite structure by cutting slabs, containing a single layer of the perovskite structure, terminating on a ⟨100⟩ surface, and replacing the methylammonium cation with butylammonium. The structure can also be considered an analogue to that of La_2CuO_4,[22] with the CuO_2 sheets replaced by MI_2 sheets and the inorganic La_2O_2 "rock salt" layers replaced by organic $(C_4H_9NH_3)_2I_2$ layers.

In $(C_4H_9NH_3)_2MI_4$, with M = Ge, Sn, Pb, the group IV cations are formally in a divalent state and therefore have a pair of nonbonding electrons in their outer electronic configuration. Typically, this lone pair of electrons results in a lowering of the coordination symmetry around these cations, for example, to a trigonal or square-pyramidal arrangement. In $(C_4H_9NH_3)_2GeI_4$, the stereochemical activity of the Ge(II) nonbonding electrons is apparent from the distorted

(22) Longo, J. M.; Raccah, P. M. *J. Solid State Chem.* **1973**, *6*, 526.

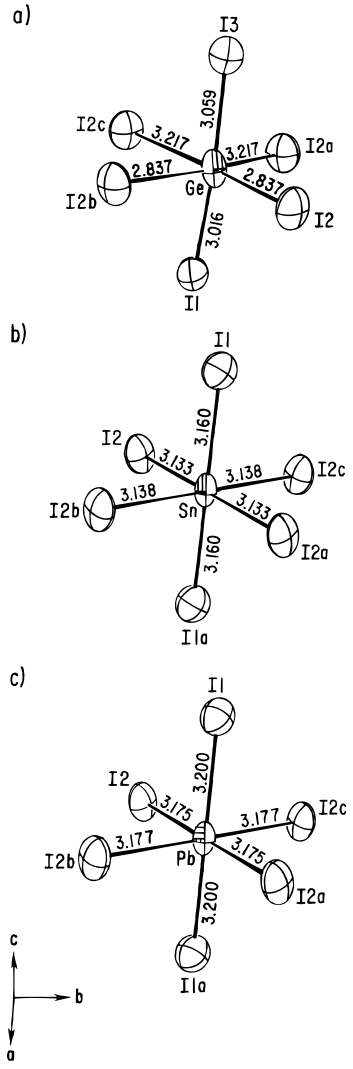

Figure 2. ORTEP drawings of the (a) GeI_6, (b) SnI_6, and (c) PbI_6 octahedra showing atom labeling, bond lengths, and anisotropic thermal ellipsoids. The ellipsoids are drawn at 50% probability.

octahedral coordination of iodines (Figure 2a), with two long and two short Ge−I(2) bonds (3.217(2) Å vs 2.837(2) Å) in the $a-b$ plane of the perovskite sheets, and two intermediate length Ge−I(1)/Ge−I(3) apical bonds (3.016(3)/3.059(3) Å) perpendicular to the sheets. Bond angles deviate significantly from 90°, with I−Ge−I bond angles ranging from 81.18(6)° to 93.36(3)°. A more complete listing of bond distances and angles in $(C_4H_9NH_3)_2GeI_4$ is given in Table 5. A similar range of Ge−I bond lengths is found in the rhombohedrally deformed room-temperature perovskite structure of $CsGeI_3$, which consists of distorted GeI_6 octahedral having three short 2.745(3) Å and three long 3.265(3) Å bonds.[20] The average Ge−I bond distance in the insulating $(C_4H_9NH_3)_2GeI_4$, 3.031 Å, is however slightly larger than in the conducting $CsGeI_3$ (3.005 Å).

The GeI_6 octahedra in $(C_4H_9NH_3)_2GeI_4$, share corners to form GeI_4 sheets. As indicated by the 166.27(8)° Ge−I(2)−Ge[d] bond angle, the octahedra alternately tilt along the a axis, producing a slight corrugation to the sheets (Figure 1). The amine nitrogens, N(1) and N(2), are located just inside the plane (along c) of the I(1)/I(3) apical iodines, with the butyl chains extending into the space between perovskite layers. The organic cations

Table 5. Selected Bond Distances and Angles in $(C_4H_9NH_3)_2GeI_4$

atoms	distances (Å)	atoms	angles (deg)
Ge−I(1)	3.016(3)	I(1)−Ge−I(2)	91.82(8)
Ge−I(2)	2.837(2)	I(1)−Ge−I(2)[a]	89.07(6)
Ge−I(2)[a]	3.217(2)	I(1)−Ge−I(2)[b]	91.82(8)
Ge−I(2)[b]	2.837(2)	I(1)−Ge−I(2)[c]	89.07(6)
Ge−I(2)[c]	3.217(2)	I(1)−Ge−I(3)	175.38(9)
Ge−I(3)	3.059(3)	I(2)−Ge−I(2)[a]	93.36(3)
I2−Ge[d]	3.217(2)	I(2)−Ge−I(2)[b]	92.08(7)
N(1)−C(1)	1.53(8)	I(2)−Ge−I(2)[c]	174.46(7)
N(2)−C(5)	1.50(6)	I(2)−Ge−I(3)	91.38(7)
C(1)−C(2)	1.2(1)	I(2)[a]−Ge−I(2)[b]	174.46(7)
C(2)−C(3)	1.5(1)	I(2)[a]−Ge−I(2)[c]	81.18(6)
C(3)−C(4)	1.1(1)	I(2)[a]−Ge−I(3)	87.43(7)
C(5)−C(6)	1.33(8)	I(2)[b]−Ge−I(2)[c]	93.36(3)
C(6)−C(7)	1.5(1)	I(2)[b]−Ge−I(3)	91.38(7)
C(7)−C(8)	1.2(1)	I(2)[c]−Ge−I(3)	87.43(7)
		Ge−I(2)−Ge[d]	166.27(8)
		N(1)−C(1)−C(2)	118(6)
		C(1)−C(2)−C(3)	112(6)
		C(2)−C(3)−C(4)	113(8)
		N(2)−C(5)−C(6)	114(4)
		C(5)−C(6)−C(7)	109(5)
		C(6)−C(7)−C(8)	111(7)

[a] $-1/2 + x$, $1 - y$, $1/2 - z$. [b] x, $1/2 - y$, z. [c] $-1/2 + x$, $-1/2 + y$, $1/2 - z$. [d] $1/2 + x$, $1 - y$, $1/2 - z$.

tilt so as to take advantage of the extra space, created by the corrugation of the inorganic sheets along the a axis, between alternate pairs of I(1) and I(3) iodines.

The $(C_4H_9NH_3)_2GeI_4$ structure is close to being A-centered (after a shift of origin). This is reflected in the (h,k,l) $k + l \neq 2n$ reflections, which are considerably weaker than other classes. The structure can, in fact, be solved in the *Abma* space group, with an R factor, R_w, that is even lower than in *Pcmn* (0.042 versus 0.051). This is misleading, however, since it is necessary to throw out close to 1800 weak, but observed (with $I/\sigma(I) > 3\sigma$), reflections (close to 25% of all reflections) in the higher symmetry solution. Comparison of the two structures reveals that the most significant deviation from A centering results from a shift of the I(2) atom in the *Pcmn* refined structure along the a axis, approximately 0.23 Å away from its ($1/4$, $1/4$, z) symmetry site in the A-centered cell (after shift of the origin). Correspondingly, the I(2) atom in the A-centered refinement has a significantly larger anisotropic thermal parameter, u_{11}, compared to that of the primitive cell (0.112(1) versus 0.083(1)). It is also principally this shift which gives rise to the significant difference between the Ge−I(2) and Ge−I(2)[a] bond lengths in the primitive refinement. In the A-centered refinement, these distances are the same (3.0240(2) Å), whereas in the primitive refinement, they are 2.837(2) and 3.217(2) Å.

Within the $(C_4H_9NH_3)_2SnI_4$ structure, which adopts the *Pbca* space group, the tin(II) iodide perovskite sheets consist of more nearly ideal octahedral tin(II) coordination (Figure 2b; Tables 6 and 7), compared with the germanium(II) compound, with two apical bond distances of 3.160(2) Å and four in-plane Sn−I(2) distances of 3.133(1) Å (2×) and 3.138(1) Å (2×). The average Sn−I bond distance, 3.144(2) Å, is somewhat larger than the six equal 3.120 Å Sn−I bonds found in the metallic cubic perovskite $CH_3NH_3SnI_3$ at room temperature.[7] The bond angles deviate moderately from 90°, with I(1)−Sn−I(2) bond angles ranging from 86.97(4)° to 93.03(4)°, resulting in alternate tilting of the apical I(1)

Table 6. Selected Bond Distances in $(C_4H_9NH_3)_2MI_4$ (M = Sn, Pb)

distances (Å)			distances (Å)		
atoms	M = Sn	M = Pb	atoms	M = Sn	M = Pb
M−I(1)	3.160(2)	3.200(2)	I(2)−M[d]	3.138(1)	3.177(2)
M−I(1)[a]	3.160(2)	3.200(2)	N−C(1)	1.64(4)	1.54(5)
M−I(2)	3.133(1)	3.175(2)	C(1)−C(2)	1.56(5)	1.45(7)
M−I(2)[a]	3.133(1)	3.175(2)	C(2)−C(3)	1.52(6)	1.5(1)
M−I(2)[b]	3.138(1)	3.177(2)	C(3)−C(4)	1.33(7)	1.1(1)
M−I(2)[c]	3.138(1)	3.177(2)			

[a] $-x, -y, -z$. [b] $1/2 - x, 1/2 + y, z$. [c] $-1/2 + x, -1/2 - y, -z$. [d] $1/2 - x, -1/2 + y, z$.

Table 7. Selected bond Angles in $(C_4H_9NH_3)_2MI_4$ (M = Sn, Pb)

	angles (deg)	
atoms	M = Sn	M = Pb
I(1)−M−I(1)[a]	180.0	180.0
I(1)−M−I(2)	91.26(4)	91.14(6)
I(1)−M−I(2)[a]	88.74(4)	88.86(6)
I(1))−M−I(2)[b]	86.97(4)	86.32(5)
I(1)−M−I(2)[c]	93.03(4)	93.68(5)
I(1)[a]−M−I(2)	88.74(4)	88.86(6)
I(1)[a]−M−I(2)[a]	91.26(4)	91.14(6)
I(1)[a]−M−I(2)[b]	93.03(4)	93.68(5)
I(1)[a]−M−I(2)[c]	86.97(4)	86.32(5)
I(2)−M−I(2)[a]	180.0	180.0
I(2)−M−I(2)[b]	88.42(3)	88.74(4)
I(2)−M−I(2)[c]	91.58(3)	91.26(4)
I(2)[a]−M−I(2)[b]	91.58(3)	91.26(4)
I(2)[a]−M−I(2)[c]	88.42(3)	88.74(4)
I(2)[b]−M−I(2)[c]	180.0	180.0
M−I(2)−M[d]	159.61(5)	155.19(6)
N−C(1)−C(2)	107(3)	108(4)
C(1)−C(2)−C(3)	98(3)	113(5)
C(2)−C(3)−C(4)	98(4)	114(7)

[a] $-x, -y, -z$. [b] $1/2 - x, 1/2 + y, z$. [c] $-1/2 + x, -1/2 - y, -z$. [d] $1/2 - x, -1/2 + y, z$.

iodines. In-plane, the I(2)−Sn−I(2) bond angles are 88.42(3)° and 91.58(3)°.

The lead(II) compound is very similar in structure to the tin(II) compound (Figure 2c; Tables 6 and 7) with an average Pb−I bond distance of 3.184 Å, which is again significantly larger than in the darkly colored though also insulating $CH_3NH_3PbI_3$, which in the cubic modification has Pb−I bond distances of 3.135 Å.[23] Progressing from the germanium(II) through the lead(II) compound, the most significant trend, with regard to bonding geometry, is a decrease in the M−I(2)−M[d] bond angle from 167.27(8)° for $(C_4H_9NH_3)_2GeI_4$ to 159.61(5)° for $(C_4H_9NH_3)_2SnI_4$ and to 155.19(6)° for $(C_4H_9NH_3)_2PbI_4$. In $(C_4H_9NH_3)_2GeI_4$, the deviation of this angle from 180° results primarily in a corrugation of the GeI_4 sheets, whereas for the tin(II) and lead(II) compounds there is both a corrugation and a rotation of the octahedra in the *a*−*b* plane (Figure 3). Also apparent from Figure 3 is the different manner in which the butylammonium cations hydrogen bond to the perovskite sheet iodines in the two structures. In $(C_4H_9NH_3)_2GeI_4$, the plane of the butylammonium cations aligns along the *a* axis, whereas in the tin(II) and lead(II) compounds, the plane of the cations is rotated approximately 45° from this axis. The organic cations also tilt more significantly away from the *c* axis in the tin(II) and lead(II) compounds, accounting for the smaller *c* lattice parameters for these systems despite the larger M−I bond lengths.

(23) Weber, D. *Z. Naturforsch.* **1978**, *33b*, 1443.

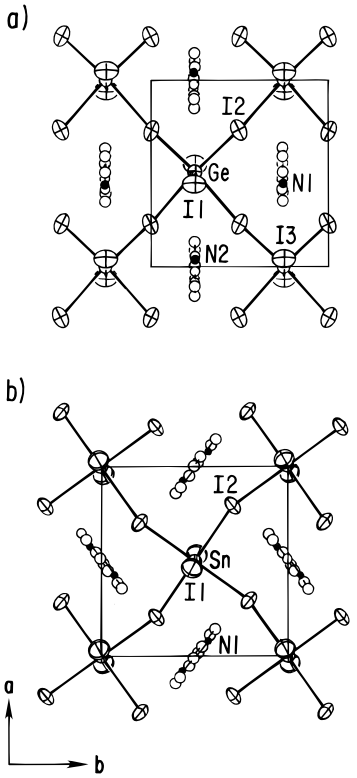

Figure 3. Single $(C_4H_9NH_3)_2MI_4$ layer, viewed down the *c* axis, for (a) M = Ge and (b) M = Sn, showing the difference in M−I(2)−M[d] bond geometry and butylammonium configuration between the two structures. The M = Pb structure (not shown) is virtually identical to that for M = Sn. The unit cell is outlined for each compound, highlighting the shift in origin in going from the *Pcmn* (for M = Ge) to the *Pbca* (for M = Sn, Pb) space group. The thermal ellipsoids for germanium, tin, and iodine are drawn at 50% probability, while carbon and nitrogen sphere sizes are arbitrary.

Stereochemical Activity of Ge(II), Sn(II), and Pb(II) Lone-Pair Electrons. The complete series $(C_4H_9NH_3)_2MI_4$, M = Ge, Sn, Pb, enables a comparison of the lone-pair activity for these divalent group IVB cations. Typically, the stereoactivity of the lone-pair electrons is significant for these cations, with the stereoactivity generally increasing in the order Pb(II) < Sn(II) < Ge(II), as bonding to the ligands becomes more covalent. For example in the insulating compounds, $[NH_2C(I)=NH_2]_3MI_5$ (M = Sn and Pb),[11] the lone-pair effect is especially pronounced for the tin(II) compound, with Sn−I bond lengths ranging from 2.957(1) to 3.484(1) Å (compared to the smaller range of bond distances, 3.153(3)−3.287(3) Å, for the lead(II) system). In the present series of single layer ⟨100⟩-oriented perovskites, $(C_4H_9NH_3)_2MI_4$ (M = Ge, Sn, Pb), the distortion of the MI_6 coordination for the germanium(II) compound is significantly more pronounced than in the tin(II) and lead(II) compounds. There is, however, very little difference in degree of distortion between the tin(II) and lead(II) compounds. For each of these materials, the M−I bond lengths are nearly identical and the biggest angular distortion from an ideal octahedral coordination involves the apical I(1) atom, with I(1)−M−I(2)[c] angles of 93.03(4)° and 93.68(5)° for the tin(II) and lead(II) compounds, respectively.

The small degree of distortion in the tin(II) compounds may be associated with its dark coloration and relatively large electrical conductivity. Absence or

reduction of the lone-pair stereoactivity is often associated with the population of an empty low-lying energy band in the solid by the nonbonding electrons, thus giving rise to optical coloration and electrical conductivity.[24] In the family of ⟨110⟩-oriented perovskites,[10,11] $[NH_2C(I)=NH_2]_2(CH_3NH_3)_mSn_mI_{3m+2}$, for example, the $m = 1$ compound is orange and insulating and has a highly distorted octahedral coordination with the six Sn−I bond lengths, 2.957(1), 3.097(2), 3.110(2), 3.267(2), 3.300(2), and 3.484(1) Å, whereas the $m = 2$ compound is very darkly colored and is semiconducting[10] and has a nearly ideal octahedral coordination with the Sn−I bond lengths, 3.094(2), 3.094(2), 3.096(3), 3.179(3), 3.185(1), and 3.185(1) Å. The black metallic cubic perovskite, $CH_3NH_3SnI_3$ ($m \rightarrow \infty$), has ideal octahedral coordination with Sn−I bond lengths of 3.120 Å. Note also that the average Sn−I bond length is significantly larger in the insulating $m = 1$ compound (3.202 Å) than in the semiconducting $m = 2$ (3.139 Å) and metallic $m \rightarrow \infty$ (3.120 Å) structures. An extended Hückel band structure calculation for $CH_3NH_3SnI_3$ indicates[10] that the metallic nature of this cubic perovskite results from the large dispersion of the Sn 5s band (hybridized with I 5p) along the ⟨111⟩ direction of the cubic Brillouin zone, leading to a marginal crossing of the Sn 5s and Sn 5p bands near the R point, $(^1/_2, ^1/_2, ^1/_2)2\pi/a$, with the Fermi energy falling roughly between the two bands. Reducing the perovskite sheet thickness (reducing m) raises the Sn 5p antibonding orbitals as well as reduces the bandwidths, leading to more semiconducting character. The apparent intimate connection between electrical conductivity, lone-pair stereochemical activity, and average Sn−I bond length in this layered perovskite family is likely to arise from this progression in electronic structure as a function of perovskite sheet thickness, as well as a possible distorting influence from the hydrogen bonding of the butylammonium cations on the adjacent perovskite sheets.

In the ⟨100⟩ series, $(C_4H_9NH_3)_2(CH_3NH_3)_{n-1}Sn_nI_{3n+1}$, the semiconducting $n = 1$ structure is reported on here and has a slightly distorted octahedral geometry with the Sn−I distances, 3.133(1), 3.133(1), 3.138(1), 3.138(1), 3.160(2), and 3.160(2) Å, and bond angles which range from 86.97(4)° to 93.03(4)°. The semimetallic $n = 3$ structure[6] has two distinct tin sites within the tin(II) iodide perovskite trilayers. The inner perovskite sheet consists of Sn(1) atoms which have a nearly ideal octahedral coordination of iodines, with two 3.123(3) Å apical bonds and four 3.127(1) Å in-plane bonds and all angles within the tin iodide octahedra 90(±1)°. The average Sn−I bond distance in this layer, 3.126 Å, is very similar to that found in the metallic $CH_3NH_3SnI_3$, while this inner layer is less distorted and has shorter Sn−I bond lengths than in the semiconducting $n = 1$ compound. The outer perovskite sheets consist of Sn(2) atoms coordinated by a much more distorted octahedra of iodines, with apical bond distances ranging from 3.003(4) Å (apical bond toward the organic layer) to 3.284(4) Å for the opposite apical bond connecting to the inner perovskite layer. The in-plane bond distances are nearly identical at 3.136(2) Å (2×) and 3.132(2) Å (2×), virtually the same as for the $n = 1$ compound. The large distortion of the SnI_6 octahedra in the outer perovskite sheets of the $n = 3$ structure is consistent with the semimetallic character of this compound if we assume that the conductivity is primarily arising from the central, nearly undistorted, perovskite sheet. Comparing the $n = 1$, $n = 3$ and $n \rightarrow \infty$ ($CH_3NH_3SnI_3$) structures, it is reasonable to associate the transition to more metallic character for $n \geq 3$ in the $(C_4H_9NH_3)_2(CH_3NH_3)_{n-1}Sn_nI_{3n+1}$ family to the appearance of less distorted central perovskite layers for $n \geq 3$, with smaller Sn−I bond distances in these layers, similar to the metallic cubic perovskite $CH_3NH_3SnI_3$.

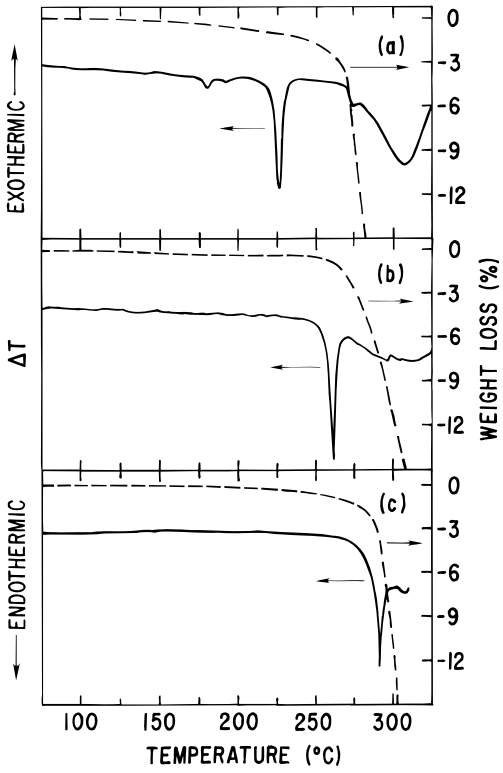

Figure 4. Simultaneous thermogravimetric analysis and differential thermal analysis scans for (a) $(C_4H_9NH_3)_2GeI_4$, (b) $(C_4H_9NH_3)_2SnI_4$, and (c) $(C_4H_9NH_3)_2PbI_4$. Each scan was performed in flowing argon with a ramp rate of 2 °C/min. For clarity, only the heating portion of the curve is shown.

Thermal Analysis. Several thermal studies on the organic−inorganic layered perovskites (in particular the Mn^{2+}, Cd^{2+}, and Cu^{2+} halide systems) have been undertaken,[25,26] demonstrating a rich array of structural transitions below the melting/decomposition point for many of these compounds. These transitions are driven primarily by order−disorder transitions of the alkylammonium cations and, for the longer alkyl chain compounds, conformational and melting transitions within the organic layer. Decomposition of the A_2MX_4 (A = organic amine, M = divalent metal, X = halogen) compounds often occurs through the simultaneous loss of A and HX from the compound below the melting temperature.[27,28]

Figure 4 shows the simultaneous thermogravimetric analysis (TGA) and differential thermal analysis (DTA)

(24) Donaldson, J. D.; Grimes, S. M. *Rev. Silicon, Germanium, Tin, Lead Compd.* **1984**, *8*, 1.

(25) Needham, G. F.; Willett, R. D.; Franzen, H. F. *J. Phys. Chem.* **1984**, *88*, 674.

(26) Vacatello, M.; de Girolamo, M.; Busico, V. *J. Chem. Soc., Faraday Trans. 1* **1981**, *77*, 2367.

(27) Tello, M. J.; Bocanegra, E. H.; Arrandiaga, M. A.; Arend, H. *Thermochim. Acta* **1975**, *11*, 96.

(28) Mitzi, D. B.; Frisch, M., unpublished.

scans for the three title group IVB metal halide compounds. For $(C_4H_9NH_3)_2GeI_4$, the main endotherm corresponds to a melting transition at 222(2) °C, which occurs significantly before the sample completely decomposes at temperatures above 270 °C. The melting transition was verified by heating a $(C_4H_9NH_3)_2GeI_4$ sample in argon and visually inspecting the sample as a function of temperature. Below 220 °C the sample was a solid pellet, while above 225 °C melting occured. Upon cooling from 230 °C, the viscous melt solidified into an orange mass of sheetlike $(C_4H_9NH_3)_2GeI_4$ crystals, demonstrating that melt-processing can be used to grow single crystals of this organic−inorganic composite material. Minor weight loss (<1%) is, however, observed in the TGA scan for $(C_4H_9NH_3)_2GeI_4$ at temperatures as low as 100 °C, most likely as a result of the loss of $C_4H_9NH_2$ and HI from the sample. A similar loss of organic material (in this case $C_3H_7NH_2$ and HBr) was directly observed using mass spectrometry and TGA on the system $(C_3H_7NH_3)_2CuBr_4$.[28] The melting temperature shifts slightly to lower temperature as the material is cycled through the melting transition, with melting temperatures reduced by as much as 4 °C (with some broadening of the endotherm) in the melt processed crystals discussed above. These observations suggest that crystals grown from the melt are likely to have defects arising from loss of butylamine and hydrogen iodide, unless excess $C_4H_9NH_2$·HI is included in the reaction vessel. The smaller endotherms starting at 175(5) °C are likely to correspond to structural transitions involving the organic cations, as has been observed in other organic−inorganic layered perovskite systems.[25,26] These transitions are reversible and also shift to lower temperature and are broadened as the materials are cycled through this temperature range and some organic material is lost.

$(C_4H_9NH_3)_2SnI_4$ (T_m = 256(2) °C) and $(C_4H_9NH_3)_2PbI_4$ (T_m = 285(4) °C) melt at progressively higher temperatures with significant decomposition at the transition, as indicated by the precipitous weight loss and the progressive growth of extra peaks in the DTA curves for these compounds as the samples are cycled through the transition. Small weight loss is observed, as for $(C_4H_9NH_3)_2GeI_4$, at temperatures as low as 100 °C, well below the bulk melting/decomposition point. In contrast to $(C_4H_9NH_3)_2GeI_4$, no other significant structure in the DTA curve is noted below the melting/decomposition transitions.

Photoluminescence. The organic−inorganic compounds $(C_mH_{2m+1}NH_3)_2(CH_3NH_3)_{n-1}M_nI_{3n+1}$ form natural multi-quantum-well structures, with variable well thickness (controlled by n), well separation (controlled by m), and even well depth (controlled by M), providing an ideal model system for tailoring optical properties. Previous work on various organic−inorganic lead(II) and tin(II) compounds has demonstrated strong luminescence in the visible range, arising from an exciton state.[12,13,16−18,29] The luminescence originates from electronic transitions within the inorganic perovskite layer, rather than from the organic layer, since the simple organic molecules being employed are transparent in the visible spectral range. In the layered lead-(II) iodide materials, the lowest exciton state arises from excitations between the valence band, which consists of a mixture of Pb(6s) and I(5p) states, and the conduction band, which derives primarily from Pb(6p) states.[30] For the tin(II) iodide materials a similar situation occurs, with a valence band derived from Sn(5s) and I(5p) origin and a conduction band having primarily Sn(5p) character.

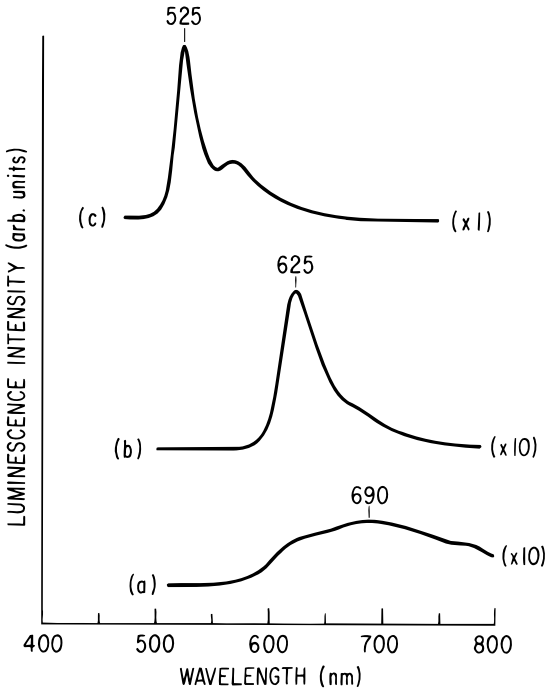

Figure 5. Photoluminescence spectra for crystals of $(C_4H_9NH_3)_2MI_4$ with (a) M = Ge, (b) M = Sn, and (c) M = Pb, demonstrating a shift in the photoluminescence peak as a function of group IVB element. Intensities for the M = Ge and Sn spectra have been multiplied by 10 to enable a more convenient comparison with the M = Pb spectrum. The photoluminescence spectra were excited by 457.9 nm light from an argon ion laser.

Ishihara et al.[12,13] have established that the very large exciton binding energy and oscillator strength in these materials are too large to be explained by the structural two-dimensionality alone and require, for an adequate explanation, a dielectric confinement effect provided by the alternation of low dielectric constant organic and high dielectric constant lead(II) iodide layers. In $(C_{10}H_{21}NH_3)_2PbI_4$, for example, the exciton state has a binding energy of 370 meV and an oscillator strength of about 0.7 per formula unit.[12] For comparison, the exciton state in PbI_2 has a binding energy of only 30 meV and an oscillator strength of 0.017. The enhancement of the exciton binding energy, provided by the unusual layered organic−inorganic structure, enables the exciton state to be very stable even at room temperature.

In the present work, we consider the room-temperature photoluminescence spectra for the single layer (n = 1) perovskites with butylammonium (m = 4) cations, to examine the effect on the luminescent properties of varying M from germanium(II) to lead(II) (Figure 5). For $(C_4H_9NH_3)_2PbI_4$, the luminescence spectra consists of a strong peak with a primary maximum at 525(1) nm and a full width at half-maximum of approximately

(29) Papavassiliou, G. C.; Koutselas, I. B.; Lagouvardos, D. J.; Kapoutsis, J.; Terzis, A.; Papaioannou, G. J. *Mol. Cryst. Liq. Cryst.* **1994**, *252−253*, 395.

(30) Ishihara, T. *J. Lumin.* **1994**, *60* and *61*, 269.

22(2) nm, while the tin(II) compound shows a significant red-shift, peaking at 625(1) nm with a larger full width at half-maximum of 38(3) nm. We estimate the luminescence efficiencies to be of order 10^{-4} for these compounds, based on a comparison of the integrated intensity under the principal photoluminescence peaks with that of the 520 cm^{-1} Raman line for bulk silicon. These results are consistent with several earlier studies on similar tin(II) and lead(II) systems[12,13,18,29] and demonstrate the ability to significantly shift, within a single structure, the luminescence spectrum by varying the electronic structure of the well material. Recently, well thickness has also been shown to have a significant impact on the optical properties. For example, in the family, $(C_6H_5C_2H_4NH_3)_2(CH_3NH_3)_{n-1}Pb_nI_{3n+1}$, the bandgap energy, the lowest exciton energy, and the exciton binding energy have all been shown to decrease with increasing sheet thickness (controlled by n) as a result of quantum confinement or dimensionality effects.[30]

The spectrum for $(C_4H_9NH_3)_2GeI_4$ is also presented in Figure 5c and has a significantly smaller peak intensity, a much larger peak width (≃180 nm), and a further red shift, with a peak center around 690(5) nm. Considerable variation in peak location and intensity was noted in the germanium(II) system, as a function of how the samples were synthesized and handled, perhaps as a result of the greater propensity for oxidation in this system. In all cases examined, however, the photoluminescence spectra for the germanium(II) system were weaker, much broader, and shifted toward higher wavelength compared to the tin(II) system. More generally, while the photoluminescence peak intensities varied somewhat from sample to sample, the peak luminescence intensity qualitatively decreased in the order M = Pb(II) > Sn(II) > Ge(II), while the peak width increased and the peak shifted toward longer wavelength. The lower room-temperature photoluminescence peak intensities most likely arise from a smaller exciton binding energy for the lighter group IVB element compounds. It has been established, for example, in the related $(C_6H_5CH_2CH_2NH_3)_2MI_4$ system, that the exciton binding energy decreases from >230 meV for M = Pb to 160−190 meV for M = Sn.[29]

In addition to the main spectral peak, there is also a higher wavelength shoulder on the $(C_4H_9NH_3)_2SnI_4$ spectrum and an additional resolved peak at higher wavelength in the $(C_4H_9NH_3)_2PbI_4$ data (at 569(2) nm). While, at present, the origin of these features is not fully understood, they appear to be enhanced somewhat by exposure to air or even storage in an argon-filled drybox for many months, suggesting that this is a surface oxidation or degradation effect. Nevertheless, even fresh crystals that have not been exposed to air exhibit these features to some extent (as seen in Figure 5). Severe exposure to air (24 h of direct contact with the ambient atmosphere) produces more pronounced degradation effects, with a dark-colored coating forming on the tin(II) samples and a light-colored coating forming on the germanium(II) samples, severely reducing the intensity of the observed luminescence. The lead(II) samples are considerably less affected by air exposure, with a comparable spectrum to that of the unexposed crystals after 24 h in air. Degradation effects have also been reported in other related organic−inorganic systems[29] and highlight the need to minimize exposure to air during the study or application of luminescence in these materials.

Conclusion

Recent interest in "tunable" materials has spurred considerable interest in the self-assembling multiquantum-well structure systems, A_2MI_4, where A represents some organic amine and M = Sn or Pb. In these systems, the semiconducting or metallic inorganic perovskite sheets represent the quantum wells, while the much larger bandgap organic layers act as barriers. In this contribution, we present an aqueous solution growth procedure for preparing a Ge(II) member of this family, $(C_4H_9NH_3)_2GeI_4$, as well as the related $(C_4H_9NH_3)_2SnI_4$ and $(C_4H_9NH_3)_2PbI_4$ compounds. Examination of the structural and physical properties of the three compounds has provided an opportunity to examine the progression of structure, as well as thermal, electrical, and optical properties of these organic−inorganic materials as a function of metal cation in the group IVB column of the periodic table.

$(C_4H_9NH_3)_2GeI_4$ is found to adopt the $n = 1$ layered perovskite structure, similar to that of $(C_4H_9NH_3)_2SnI_4$ and $(C_4H_9NH_3)_2PbI_4$, but with a different space group and greater distortion of the GeI_6 octahedra. $(C_4H_9NH_3)_2GeI_4$ melts at 222(2) °C, with some evidence in the differential thermal analysis curve for a reversible structural transition below the melting point. Progressing down the group IVB series to the Sn(II) and Pb(II) compounds, the melting temperature increases from 256(2) °C for $(C_4H_9NH_3)_2SnI_4$ to 285(4) °C for $(C_4H_9NH_3)_2PbI_4$, with more decomposition at the higher melting transitions. Whereas both the $(C_4H_9NH_3)_2PbI_4$ and $(C_4H_9NH_3)_2GeI_4$ compounds are orange and insulating, $(C_4H_9NH_3)_2SnI_4$ is dark red (almost black in reflection) and is semiconducting with a room-temperature resistivity of order 10^5 Ω cm.[6] $(C_4H_9NH_3)_2GeI_4$ exhibits very broad room-temperature photoluminescence which peaks around 690(5) nm. The photoluminescence spectra for $(C_4H_9NH_3)_2SnI_4$ and $(C_4H_9NH_3)_2PbI_4$ are more sharply peaked and progressively shift towards the blue, peaking at 625(1) and 525(1) nm, respectively.

As for the Sn and Pb systems, which demonstrate considerable flexibility to replace butylammonium with a wide variety of other organic amines, we expect that the Ge(II) system will exhibit similar flexibility. The ability to substitute a wide range of organic molecules should enable some degree of control over physical properties such as luminescence and conductivity. Furthermore, we expect that as for the Sn(II) system, $(C_4H_9NH_3)_2(CH_3NH_3)_{n-1}Sn_nI_{3n+1}$, in which the thickness of the perovskite sheets is controlled by varying n, it should also be possible to grow multilayer Ge(II)-based perovskites. To demonstrate this, we have recently grown, using a similar technique as described in this paper, the Ge(II) analogues, $(C_4H_9NH_3)_2(CH_3NH_3)_{n-1}Ge_nI_{3n+1}$, $n = 2$ and 3. The color of these higher n members darkens with increasing perovskite sheet thickness, suggesting that the bandgap decreases with increasing n. We have also synthesized the $n = 2$ compound with the methylammonium cation replaced by cesium. The cesium series is particularly interesting given the metallic character of the $n \rightarrow \infty$ end-member, $CsGeI_3$. The flexibility to chose the metal cation (Ge, Sn, or Pb), organic cation, and thickness of the perovs-

kite sheet is expected to provide a rich opportunity to study quantum effects in layered systems and may also enable the design of technologically important materials.

Finally, the $(C_4H_9NH_3)_2MI_4$ (M = Ge, Sn, Pb) family provides an ideal opportunity to consider the M(II) lone-pair effect for the group IVB metal atoms. The lone-pair stereoactivity for the group IVB elements in these structures is significant in the Ge(II) compound but weak in the Sn(II) and Pb(II) compounds. The reduction of lone-pair stereoactivity in the tin(II) compound is likely to be associated with a solid-state effect in which the lone-pair electrons are contributed to a conduction band. Comparison of the semiconducting $n = 1$, the semimetallic $n = 3$, and the metallic $n \rightarrow \infty$ structures in the family, $(C_4H_9NH_3)_2(CH_3NH_3)_{n-1}Sn_nI_{3n+1}$, demonstrates that there is an intimate connection between the perovskite sheet thickness, the Sn(II) lone-pair stereoactivity, the average Sn−I bond lengths, and the electrical conductivity of these compounds. Metallic conduction is associated with inactivity of the Sn(II) lone pair and shorter Sn−I bond lengths (≃3.120 Å), while semiconducting behavior is correlated with lone-pair activity and longer average Sn−I bond lengths.

Acknowledgment. The author wishes to thank S. Wang, S. La Placa, C. A. Feild, and B. A. Scott for stimulating discussions and J. C. Tsang for performing the photoluminescence measurements.

Supporting Information Available: Tables showing anisotropic temperature factors for the germanium, tin, and lead compounds (1 page). This material is contained in many libraries on microfiche, immediately follows this article in the microfilm version of the journal, and can be ordered from the ACS; see any current masthead page for ordering information.

CM9505097